Manuscript Click here to view linked References

Biochemical and Biophysical Features of Mutated Tau Proteins V363A and V363I

Ada De Luigi[a], Laura Colombo[a], Luca Russo[a], Caterina Ricci[b], Antonio Bastone[a], Sara Cimini[c], Fabrizio Tagliavini[c], Giacomina Rossi[c], Laura Cantù[d], Elena Del Favero[d]*, Mario Salmona[a]*

[a] Department of Molecular Biochemistry and Pharmacology, Mario Negri Institute of Pharmacological Research IRCCS, Milano, Italy

[b] Department of Biosciences, University of Milan, Milano, Italy

[c] Unit of Neurology V and Neuropathology, Fondazione IRCCS Istituto Neurologico Carlo Besta, Milano, Italy

[d] Department of Medical Biotechnology and Translational Medicine, University of Milan, LITA, Segrate (Milano), Italy

*Correspondence to:

Elena Del Favero elena.delfavero@unimi.it Department of Medical Biotechnology and Translational Medicine, University of Milan, LITA V.le F.lli Cervi 93, 20090 Segrate, Italy, Tel +39 02 5033 0351

Mario Salmona mario.salmona@marionegri.it Department of Molecular Biochemistry and Pharmacology, Mario Negri Institute of Pharmacological Research IRCCS, Via Mario Negri 2, 20156 Milano, Italy, Tel +39 02 3901 4447

Highlights

- Point mutations in P301L, V363A and V363I do not induce crucial changes in the folding of free monomeric tau in solution.
- Interaction with heparin provides P301L, V363A and V363I tau variants with complexes of different shape
- V363A and V363I tau show aggregated intermediates with altered persistence, morphology and hydrophobic exposure in mid and long times
- V363A and V363I tau exhibit different cell toxicity profiles in short and long times

Abstract

Comprehension of the pathogenetic mechanisms in tauopathy-associated neurodegenerative diseases may be improved by knowledge of the biochemical and biophysical features of mutated tau proteins. Here, we used the full-length wild-type tau, the V363A and V363I mutated species, associated to pathology, and the P301L mutated tau, as a benchmark. With a pool of techniques, including small angle X-ray scattering, atomic force microscopy, thioflavin T binding, and electrophoretic separation, we compared their course from intrinsically disordered monomers in solution to early-stage recruitment in complexes and then aggregates of increasing size over long times up to the asymptotic aggregative behavior of full-length tau proteins. We show that diversity in the kinetics of recruitment and aggregate structure occurs from the very start, and spreads all over their pathway to very large objects. The different extent of conformational changes and types of molecular assemblies among the proteins were also reflected in their *in vitro* toxicity; this variation could correlate with physiopathology in humans, considering that the mutation P301L is more aggressive than V363A and especially V363I. This study identified the presence of aggregation intermediates and corroborated the oligomeric hypothesis of tauopathies.

Keywords: tau protein, tauopathy, mutation, aggregation, oligomers, fibrils

Abbreviations: CD, circular dichroism; SAXS, small-angle X-ray scattering; ThT, thioflavin T; $t_{1/2,}$ half-time; AFM, atomic force microscopy; ANS, 8-anilino-1-naphthalene sulfonic acid; MTT, methylthiazolyldiphenyl-tetrazolium bromide.

1. Introduction

The microtubule-associated protein tau can form neurofibrillary tangles, which are hallmarks of several neurodegenerative diseases termed tauopathies. In many instances, this pathological feature is considered to represent secondary amyloidosis, which shares a common mechanism with Alzheimer's disease, Parkinson's disease, and dementia with Lewy bodies [1]. In tauopathies, such as frontotemporal lobar degeneration, the deposition of abnormal tau fibrils is the primary contributing factor to neuronal death and brain atrophy [2]. Tau is, therefore, considered to be a potential therapeutic target for the treatment of tauopathies.

Tau is encoded by the *MAPT* gene and plays several physiological roles in neurons, including mediating intracellular trafficking and regulating neurite outgrowth, synaptogenesis, and plasticity. Under certain conditions, the inability of tau to perform its normal functions leads to defective myelination, dendritic spine alterations, and enhanced glutamatergic transmission [3].

Misprocessing of tau represents a potential route of toxicity, either through intracellular alterations in the unfolded protein system that regulates protein degradation (proteasomes and chaperones) or through extracellular secretion of source seeds for aggregation (transcellular release, microvesicles, or exosomes), which has been widely described [4].

Tau is an intrinsically disordered and highly soluble protein with a sizeable unstructured region and a small region that forms β-sheets [5]. Several studies have demonstrated that the microtubule-binding portion of tau (243-372 aa) is fundamental to the assembly process (due to intra- and intermolecular interactions mediated by disulfide linkages); variations in the cytoplasmic environment (e.g., reducing status, buffered conditions, and altered concentration of polyanions) that occur due to aging or neurodegenerative conditions can promote the initial phase of tau polymerization (nucleation–elongation) and sustain the progression of aggregation [6,7].

Under physiological conditions, tau has a low propensity to self-organize into toxic aggregates. Although the mechanism that triggers aggregation remains unclear, studies have demonstrated that tau mutations are often crucial to the transition from monomeric to aggregated forms because mutant tau displays a higher propensity to self-aggregate into oligomers [8]. The P301L mutation leads to preferential deposition of four microtubule-binding repeat tau isoforms in the brain, and this mutation

results in disease development during mid-life, characterized by rapid progression and severe pathology [9].

Tau oligomers are considered to be the most toxic tau species and cause tauopathy progression [10]. Among the numerous tau mutations described in the literature, the V363A and V363I mutations were discovered in patients suffering from uncommon frontotemporal lobar degeneration with peculiar pathological phenotypes [11–13]. These mutations, which result in the replacement of valine with either alanine or isoleucine, have differing effects on tau's ability to promote polymerization of tubulin and form fibrils, favoring an oligomeric form [12].

Tau has been shown to recruit other isoforms, which extends the core fibril structure with paired helical and straight filaments, resulting in seeding and spreading of tau oligomers which likely represent a fundamental aggregation intermediate that may be vital to the spread of disease [10,14,15]. Considering these facts, studying the aggregative process of tau may help understand the crucial factors underlying mechanisms of toxicity.

The assembly of tau oligomers is not phosphorylation-dependent, and *in vitro* experiments using various assays have demonstrated that aggregation may occur autonomously. Whether phosphorylation is fundamental to tau polymerization or whether oligomerization can occur independently remains to be determined [16].

This study examined the different molecular assemblies formed by full-length wild-type (WT), P301L, V363A, and V363I tau interacting with the polyanionic cofactor heparin to gain deeper insight into the mechanism underlying the transition from intrinsically disordered monomers to structured forms of tau. We conducted experiments using recombinant human tau protein isoform 2N4R, which was not subjected to any physicochemical processes such as centrifugation, sonication, and cross-linking [17–23]. A variety of biophysical and biochemical approaches were used to investigate features of mutated V363A and V363I from monomeric status, to molecular interactions with heparin, to small complexes, to structural evolution of assemblies across long incubation times.

2. Materials and Methods

2.1 Production of recombinant tau proteins

All tau proteins were expressed and purified as described in previously published protocols [12]. cDNA of the 441 amino acid tau isoform (2N4R) was cloned into the pRK172 bacterial expression vector and subjected to site-directed mutagenesis (QuikChange XL, Stratagene), which changed the valine at position 363 to either isoleucine (GTC to ATC) or alanine (GTC to GCC); the P301L mutation (CCG to CTG) was also produced to act as a mutated positive control. WT and mutated tau proteins were expressed in BL21(DE3) *Escherichia coli* (Novagen, Merck KGaA) cells by using isopropyl-β-D-thiogalactopyranoside (1 mM for 2.5 h). The bacteria were pelleted, resuspended in lysis buffer (20 mM 1,4-piperazinediethanesulfonic acid, pH 6.8, 1 mM ethylene glycol-bis-2-aminoethylether-N, N, N′,N′-tetraacetic acid, 1 mM DTT, and a protease inhibitor cocktail Roche), and sonicated. After centrifugation, the pellets were re-lysed.

All supernatants were incubated with benzonase (Merck, 25 U/ml, 5 mM $MgCl_2$) at 37°C for 3 h, boiled for 10 min, and centrifuged to separate the heat-denatured proteins. The supernatant was filtered (0.45 µm), loaded onto a Mono S 5/50 GL cation exchange column (GE Healthcare), and the fractions were eluted with a linear gradient (0%–100% 0.75 mM NaCl, 50 mM 4-morpholine ethanesulfonic acid, pH 6.25 and 1 mM DTT). Fractions containing the highest protein concentrations were determined by sodium dodecyl sulfate-polyacrylamide gel electrophoresis (SDS-PAGE) and pooled. Pure tau was passed over a PD-10 column (Sephadex G-25M, Merck) by using a phosphate buffer (PB, 5 mM, pH 7.4, containing a protease inhibitor cocktail, Roche), and concentrations were determined by densitometric analysis of Coomassie blue-stained SDS-PAGE gels by comparing them against concentrations of commercial tau protein, which was used as a standard (ab84700, Abcam).

2.2 Circular dichroism (CD) spectroscopy

Tau proteins were analyzed immediately after dilution to a final concentration of 2.7 µM in 50 mM PB (pH 7.4). The CD spectra were recorded on a Jasco J-815 spectropolarimeter (Jasco) at 4°C from 195 to 260 nm (1.0 nm bandwidth and 0.1 nm resolution) by using a 0.1-cm path length quartz cell. Generally, sensitivity was 100 mdeg, with a response of 4 s and a scan speed of 50 nm/min,

and five accumulations were used. CD spectra were expressed as the mean molar ellipticity after subtracting the spectrum for PB alone.

2.3 Small angle X-ray scattering (SAXS)

SAXS experiments were performed at the ESRF synchrotron (Grenoble, France) with beamline BM29. The SAXS profiles report the scattered radiation intensity as a function of the momentum transfer: namely, $q = (4\pi/\lambda) \sin(\theta/2)$, where θ is the scattering angle and λ is the beam wavelength. The intensity spectra were analyzed to obtain information regarding the particles' size and shape in solution [24].

The low-resolution shapes were reconstructed using the experimental curve and the pair-distance distribution function $P(r)$ as input, which was calculated using the indirect Fourier transform method implemented in the program GNOM, which is included in the ATSAS package [25]. For *ab initio* reconstruction, the program GASBOR uses the $P(r)$ function and considers a chain-like ensemble of dummy residues that best fit the experimental data. After checking for outliers with low normalized spatial discrepancy by using DAMSEL, the validity of the solution was supported by averaging 20 independent reconstructions with DAMAVER. All figures of cartoon and surface models were generated in PYMOL (The PyMOL Molecular Graphics System, version 2.4.0a, Schrödinger, L. L. C.).

2.4 Tau aggregation

Tau proteins (20 µM in 50 mM sterile PB containing 1 mM DTT) were heated at 50°C for 5 min to completely reduce the monomer, an anionic inducer was added (230 µg/ml heparin, 18 kDa, Sigma), and aliquots of the solution were incubated at 37°C for different times (0, 1, 3, and 6 h and 1, 2, 3, 4, 7, 14, 21, and 28 days, depending on the experiment). Under these conditions, the spontaneous aggregation of tau proteins was detectable by electrophoretic separation, microscopy analysis, the presence of β-sheet structures, and protein folding assays. The biological effects of these incubations were also determined in a cell-based assay.

2.5 Thioflavin T (ThT) binding assay

To follow the progression of β-sheet formation, tau proteins were diluted to 10 µM in 50 mM sterile PB containing 1 mM DTT and heated at 50°C for 5 min. The solution was then aliquoted into black-walled 96-well plates (cc3631, Corning) in triplicate, and heparin (115 µg/ml) and ThT (20 µM, Sigma) were added. Plates were sealed, and fluorescence (excitation 448 nm and emission 485 nm) was measured every 15 min for 96 h with an Infinite F500 plate reader (Tecan) at 37°C without shaking. Data were calculated by subtracting the fluorescence value of the solution without protein (PB + DTT + heparin + ThT) from each emission curve, and values were expressed as the mean ± standard error. The half-time of transition ($t_{1/2}$) was calculated as the time required to reach 50% of the maximal amplitude, and these values were obtained by normalizing the ThT traces on the corresponding maximal ThT fluorescence intensity. In the absence of the anionic inducer heparin, no changes in fluorescence were detected for any of the tau proteins (data not shown).

2.6 Semi-denaturing gel electrophoresis

To verify the formation of molecular assemblies, 2 µg of each tau protein from each time point was separated in 2.5% stacking and 8% resolving polyacrylamide gels. Sample loading buffer (25 mM Tris, 200 mM glycine, 0.2% SDS, 5% glycerol, and 0.025% bromophenol blue) was added to each sample and incubated for 7 min at room temperature before loading. After electrophoresis, the gels were stained with R-250 Coomassie blue (0.25%, 60 min, Sigma) and de-stained with 30% methanol and 10% acetic acid overnight, followed by image acquisition (ChemiDoc, Bio-Rad).

2.7 Atomic force microscopy (AFM) analysis

We used AFM to visualize the formation of molecular assemblies during the spontaneous aggregation of tau protein. Tau protein solutions were prepared and incubated as described for aggregation studies and diluted to 1 µM with 50 mM PB. 30 µl of each sample was spotted onto freshly cleaved muscovite mica disks (Assing) and incubated for 5 min. The mica disks were then washed with 5 ml Milli-Q water and dried under a gentle nitrogen flow. Measurements were performed using 0.01–0.025 Ohm/cm antimony-doped silicon probes (T: 3.5–4.5 µm, L: 115–135

µm, W: 30-40 µm, k: 20–80 N/m, f_0: 323–380 kHz, Bruker AFM probes) on a Multimode AFM with a Nanoscope V system operating in tapping mode with a scan rate in the 0.5–1.2 Hz range, proportional to the area scanned. Measurements confirmed all topographic patterns on at least three separate areas. To exclude the interference of artefacts, freshly cleaved mica soaked in 30 µl 50 mM PB and containing 1 mM DTT and 11.5 µg/ml heparin were also analyzed as controls. To describe the aggregated structures, AFM sample images were analyzed for diameter and height with the Scanning Probe Image Processor (SPIP Version 5.1.6) data analysis package.

2.8 1-Anilino-naphthalene-8-sulfonic acid (ANS) assay

To verify the propensity for hydrophobic conformational changes, tau proteins incubated for different times were diluted in 50 mM sterile PB to a final concentration of 2 µM. The solutions were aliquoted into black-walled 96-well plates (cc3631, Corning) in triplicate, and 20 µM ANS (Life Technology) was added. Fluorescence (excitation 375 nm and emission 460 nm) was read by an Infinite M200 plate reader (Tecan). Data were calculated by subtracting the solution's fluorescence without protein (PB + DTT + heparin + ANS) from each emission value, and values were expressed as the mean ± standard error of eight replicates from two different experiments. Statistical differences were calculated using GraphPad Prism 7.0. One-way analysis of variance (ANOVA) and Dunnett's multiple comparison test were used to assess whether differences were statistically significant. In the absence of the anionic inducer heparin, no changes in fluorescence were reported for any tau protein (data not shown).

2.9 Methylthiazolyldiphenyl-tetrazolium bromide (MTT) assay

To assess the biological effects of tau proteins after different incubation times, human neuroblastoma SH-SY5Y cells were seeded in a 96-well plate (10^5 cells/ml) in Dulbecco's modified Eagle's medium (DMEM, Lonza) supplemented with 5 mM L-glutamine (Gibco), antibiotics (10,000 U penicillin/streptomycin, Lonza), and 10% heat-inactivated fetal calf serum (FCS, Gibco). After complete plating (37°C in a humidified 5% CO_2 atmosphere), the medium was replaced with 1% FCS in DMEM to reduce cell growth. Tau proteins incubated for different times were added to each

well to a final concentration of 1 µM, and the SH-SY5Y cells were treated for 24 h. Cell viability was assessed by the direct measurement of mitochondrial activity by using the MTT reduction assay. Tetrazolium solution (20 µl of a 5 mg/ml stock solution, Sigma) was added to each well and incubated for 4 h. The medium was replaced with acidified isopropanol (0.04 M HCl) to dissolve the purple precipitate, and the absorbance intensity was measured at 570 nm by using a plate reader (Infinite M200, Tecan). Data were expressed as the percent control (PB + DTT + heparin), and values are expressed as the mean ± standard error for 10 replicates from three independent experiments. Statistical differences were calculated by using GraphPad Prism 7.0. One-way ANOVA, and Dunnett's multiple comparison test were used to assess whether differences were statistically significant.

3. Results

3.1 Point mutations in P301L, V363A and V363I do not induce crucial changes in the folding of monomeric tau in solution

To assess the initial status of tau, we used circular dichroism (CD) spectroscopy to examine each protein at the same solution concentration (2.7 µM), as determined by densitometric quantification of purified proteins (Fig. 1). WT tau's spectrum overlapped with the spectra of P301L, V36A, and V363I mutated proteins, indicating that all proteins demonstrated the same tendency toward an unfolded random structure. This result served as the starting point for subsequent experiments.

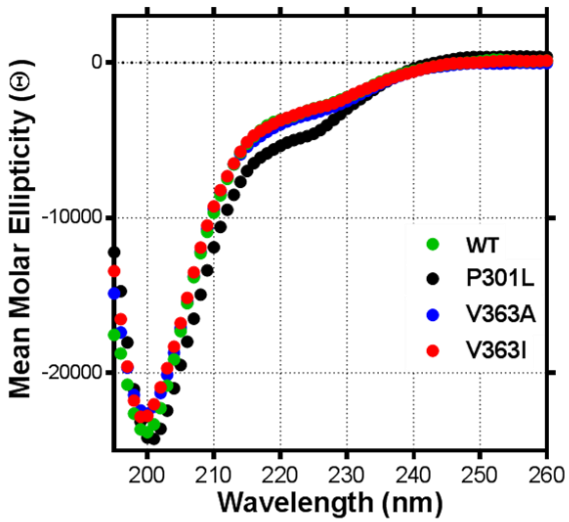

Figure 1. Circular dichroism spectra of WT and mutated tau proteins (2.7 µM). Molar ellipticity was determined from 195 to 260 nm in the absence of heparin.

To assess the size and overall conformations of free-standing monomeric proteins in buffer solution, we performed small-angle x-ray scattering (SAXS) experiments on the different tau proteins (27 µM) directly after dissolution. Figure 2A depicts the scattered intensity profiles I(q) of the different tau proteins, vertically shifted for better visibility. The corresponding Kratky plots [Fig. 2B, $q^2I(q)$ vs. q] display plateaus at $q < 1$ nm^{-1}, followed by a slight positive slope at high q values. This behavior excludes species with a globular spatial arrangement and is instead more typically observed for Gaussian chains or unfolded proteins [26]. Similar behavior has been reported for WT tau species at higher concentrations (2–10 mg/ml) [27,28]. The calculated radius of gyration (Rg values) of each protein is reported in Table 1. Values are also consistent with the expected size of monomeric tau protein for the mutated proteins, with P301L displaying the more compact spatial arrangement.

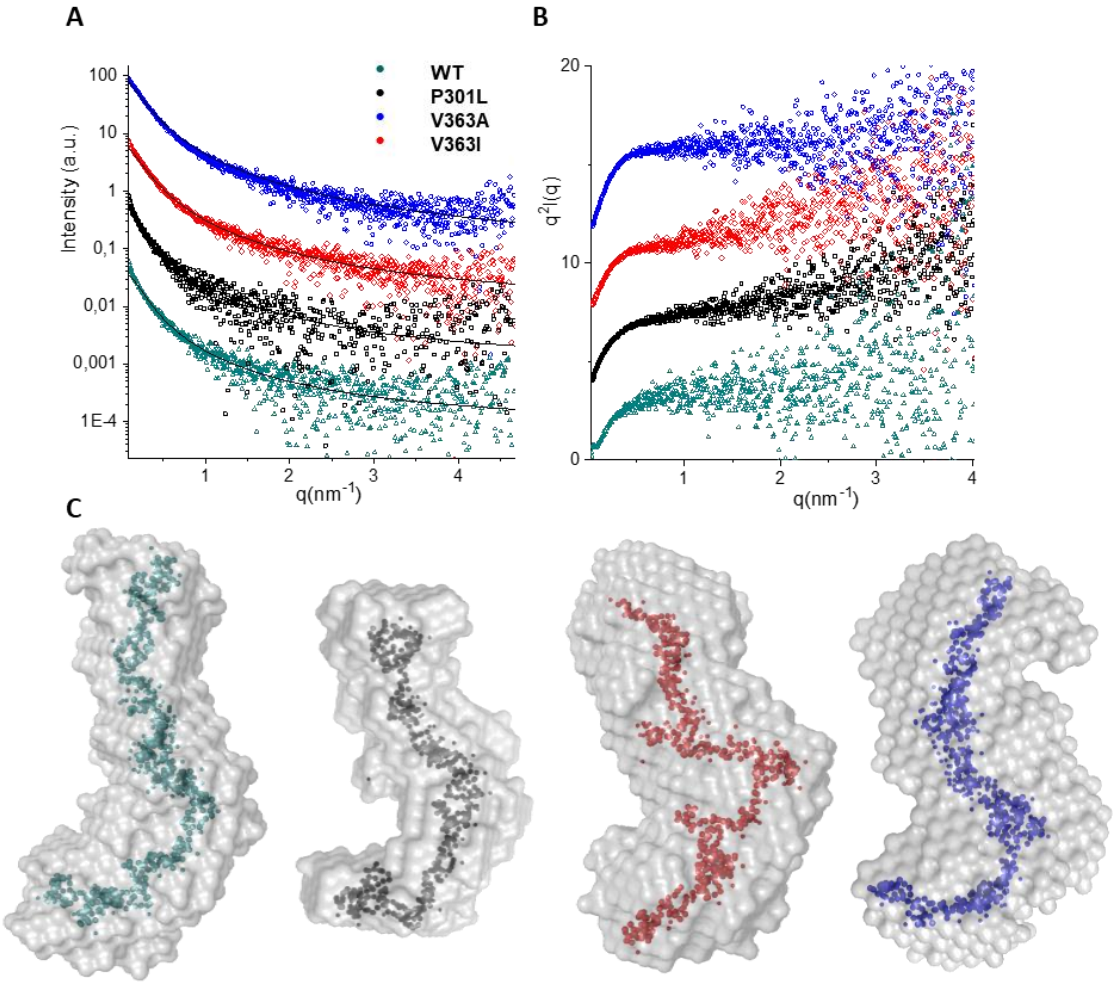

Figure 2. SAXS results for WT and mutated tau proteins (1.5 mg/ml, 27 µM). (**A**) Experimental scattered intensity (symbols) with the corresponding fit (—) for tau WT, P301L, V363I, and V363A. The spectra are vertically shifted for better visualization. (**B**) Kratky plot, $q^2I(q)$, corresponding to data reported in panel A. (**C**) *Ab initio* low resolution shape reconstruction for WT and P301L, V363A, and V363I mutations calculated from SAXS data by using GASBOR. The three-dimensional models in gray represent the probability map obtained from the average of 20 reconstructions. The characteristic structure of each protein is depicted in the same color code as the corresponding SAXS curve.

Ab initio modelling was performed and tested on the SAXS profiles to reconstruct the low-resolution spatial arrangement of proteins in solution, starting from the fitting of the curve and the interatomic

distance distribution functions P(r) (Fig. S1 and S2). The reconstructed three-dimensional hindrance models of the four considered tau variants are reported in Fig. 2C. For each variant, the characteristic structure is highlighted with the same color code as the corresponding SAXS curve. The probability map is represented in grey around each reconstruction. The results confirmed the unfolded state of all proteins, with a splayed conformation for WT tau and a more compact outline for the P301L variant. V363A and V363I mutated tau display an intermediate spatial arrangement. Each tau species behaves as an intrinsically disordered protein in buffer solution, and no crucial changes in tau monomers folding were induced by the considered point mutations.

Table 1: Gyration radii of WT and mutated tau proteins in solution in the absence and presence of heparin.

Tau protein	Rg (nm) *without heparin*	Rg (nm) *with heparin*
WT	9.6 ± 0.3	12.3 ± 0.5
V363A	7.2 ± 0.2	8.0 ± 0.3
V363I	7.6 ± 0.2	8.6 ± 0.2
P301L	6.8 ± 0.2	15 ± 1

3.2 First-step complexation with the anionic inducer heparin provides tau variants with seeds of different shape

SAXS measurements were performed on solutions containing either WT or mutated tau in the presence of the anionic inducer heparin (18 kDa) at a 1:1 molar ratio directly after mixing. Both the Rg values (Table 1) and the Kratky plots (Fig. 3A) revealed that interactions between tau and heparin readily occurred in all cases, inducing complexation. However, different features were observed for the different tau species.

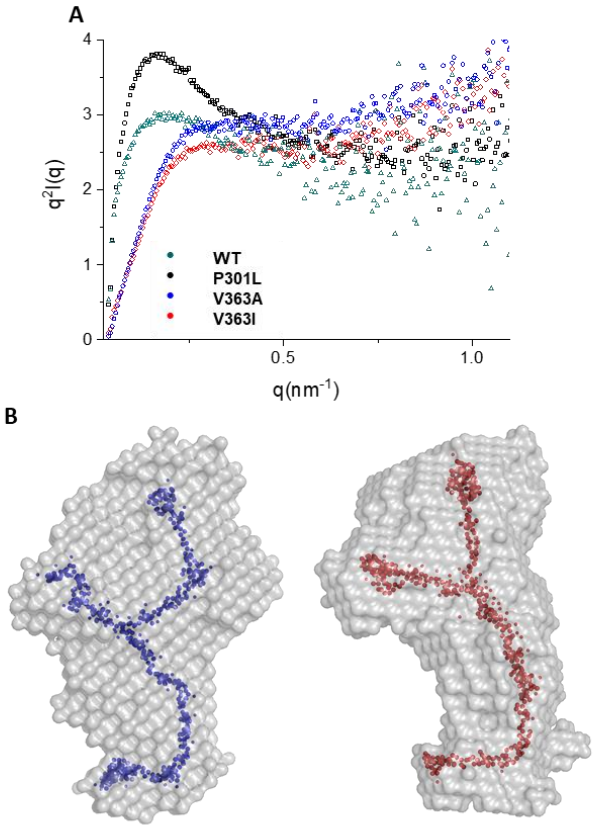

Figure 3. (**A**) Kratky plots of the SAXS intensities scattered by solutions containing the different tau mutations immediately after mixing with heparin (1:1 molar ratio). (**B**) *Ab initio* models of V363A and V363I (in blue and red, respectively) calculated from SAXS data using GASBOR. The three-dimensional models in gray represent the probability map obtained from the average of 20 reconstructions. The characteristic structure is depicted in the same color code as the corresponding SAXS curve.

Upon addition of heparin, the WT species formed complexes with a Rg value of 12 nm with a tendency towards a globular shape, as depicted by the change of the corresponding Kratky plot toward an approximately bell-shaped curve. Results suggest the presence of polydisperse species, from monomer to low-weight complexes, as shown from the low-q intensity profile in Fig. S3. P301L was the protein most prone to complex with heparin, with a Rg value of 15 ± 1 nm and a bell-shaped Kratky plot. It also had a higher maximum, indicating that a large fraction of P301L monomers

interacted with heparin chains to form low-weight complexes (see also Fig. S4). In contrast, complexation of the V363I and V363A isoforms with heparin did not induce transition to a globular shape. The average sizes of the particles in solution increased slightly (Rg values of 8.6 and 8.0 nm for V363I and V363A, respectively); however, the Kratky plots showed a plateau, indicating that the proteins were unfolded. *Ab initio* reconstructions for V363I and V363A suggest one-to-one complexation of heparin chains with mutated tau (Fig 3B). Complexation appears to involve a restricted segment of the protein chain as the strongly negatively charged heparin easily binds to positively charged lysine and arginine residues [29,30]. The anionic heparin chain may protrude from tau protein like a hook, thus promoting bridging with other monomers or cationic sites.

3.3 V363A and V363I tau aggregate with different kinetics

We used thioflavin T (ThT) fluorescent binding dye to evaluate differences in formation of β-sheet structures and aggregation kinetics among the various tau mutations (Fig. 4A). ThT and heparin (20 μM and 115 μg/ml respectively) were added to 10 μM tau protein solutions, and fluorescence was detected every 15 min for 96 h at 37°C. Samples were also collected for electrophoretic separation to determine species assembled at each time point. More pronounced β-sheet formation was evident for tau mutated proteins compared with WT tau (Fig. 4A). At the same concentrations, P301L tau promptly formed β-sheet structures with no detectable lag time, a distinctive shape, and a half-time ($t_{1/2}$) of 4 h. On the other hand, WT tau was slower ($t_{1/2}$ = 9 h) and less efficient in forming a structured β-sheet, as evident from the tenfold lower detected fluorescence intensity. V363A and V363I tau were effective at forming β-sheet structures, as shown by the fluorescence twofold more intense than WT tau; however, they had threefold less intensity than P301L tau. Moreover, the V363 mutated forms demonstrated the slowest conformational change to β-sheet structure with a $t_{1/2}$ of 10 h.

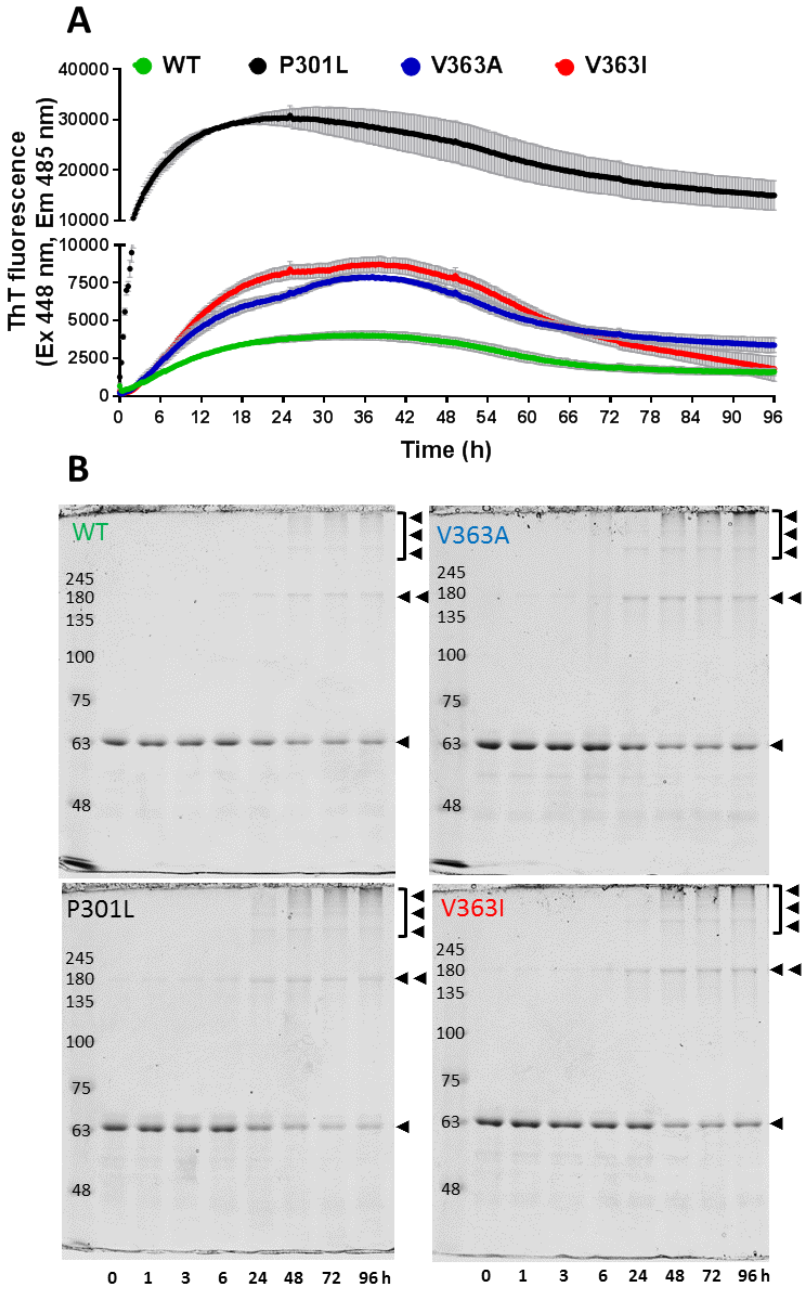

Figure 4. Aggregation of mutated tau proteins. (**A**) Thioflavin T (ThT) binding analysis. Kinetics of ThT (20 µM) fluorescence emission following incubation with WT and mutated tau proteins (10 µM) at 37°C for 96 h in presence of heparin. Data represent the mean ± SE of three replicates. (**B**) Semi-denaturing PAGE analysis of samples obtained during the aggregation process; 2 µg of protein/lane of WT and mutated tau proteins were resolved in 8% polyacrylamide gels and stained with R-250 Coomassie blue. The first lane reports the molecular markers (MW, kDa). The following symbols are used: ◄ monomers (apparent MW 63 kDa), ◄◄ oligomers (apparent MW 180 kDa), and ◄◄◄ large aggregates (apparent MW > 245 kDa).

During aggregation, the different species were characterized by semi-denaturing gel electrophoresis (Fig. 4B). Initially, all tau proteins existed in monomeric form with an apparent molecular weight close to the 63 kDa standard protein marker. After 3 h of incubation, P301L, V363A, and V363I proteins displayed bands close to the 180 kDa marker, which became more pronounced after 6 h. After 24 h, the concentration of the monomeric forms decreased and the higher molecular forms (180 and >245 kDa) increased for all tau proteins, including WT tau. On the second, third, and fourth days, the monomeric form further diminished, while the aggregated and larger forms continued to increase, with sizes that reached the edge of the resolving gel; larger forms appeared to occur more markedly for mutant tau than for WT tau.

3.4 V363I and V363A mutated tau displayed peculiar morphological and biochemical features

To investigate molecular assembly progression of the mutated tau proteins over a prolonged incubation time, we used the same experimental interval conditions for AFM and electrophoretic experiments. Figure 5 illustrates the time of course of tau protein aggregation by atomic force microscopy (AFM). All examined tau proteins appeared to be unstructured, with a few round structures that were 20–30 nm in diameter at zero time. WT tau maintained a low propensity to form structured assemblies throughout the kinetic experiment, with little amorphous material and a tendency to coordinate water. P301L started after 6 h to form protofibrils and short fibrils in coexistence with 20–30-nm diameter structures. The protofibrils evolved into fibrils, reaching lengths of up to 9 µm while preserving a fraction of less-structured aggregates with diameter of 20–100 nm. V363A and V363I tau both tended to form fibrils, but with slower kinetics than P301L tau. At 6 h, both V363A and V363I proteins appeared to contain large amounts of amorphous material, which evolved into structured fibrils (9 – 10 µm in length), in coexistence with less-structured complexes; these were present in lower amounts compared with P301L at all incubation times. Results suggested that V363I tau followed a delayed fibril formation in comparison with V363A tau, which already showed protofibrillar structures (up to 500 nm) at 6 h.

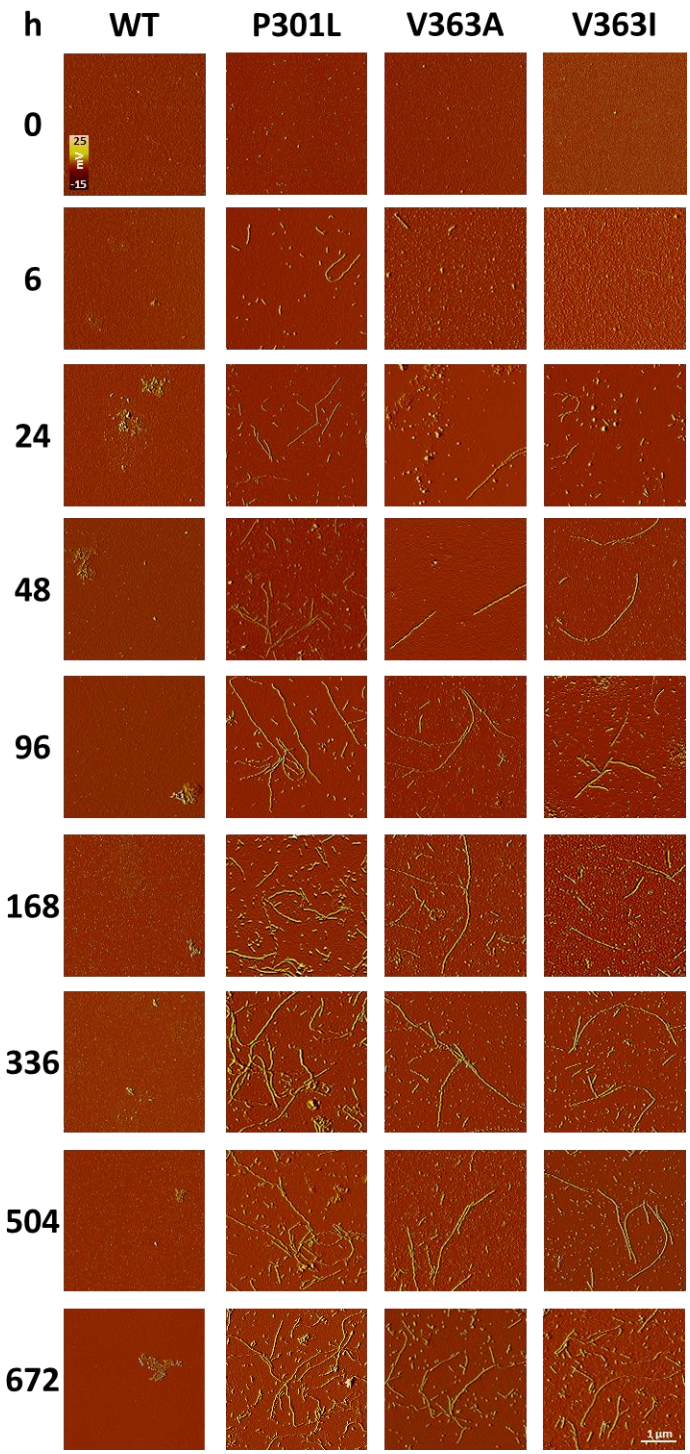

Figure 5. AFM analysis of tau proteins at different incubation times. WT and mutated tau proteins (1 µM) were observed after incubation at 37°C for different intervals of time in presence of heparin. Scale bar, 1 µm. Topographic amplitude errors are indicated by the color bar.

Electrophoretic separation after 96 h of incubation demonstrated the persistence of transitory intermediate forms (~180 kDa) for all mutated tau. Figure 6A depicts the disappearance of

monomeric forms of all tau proteins at long incubation times; this occurred sooner for P301L and V363I tau, with evident conversion of monomeric and intermediate forms into larger aggregates after 168 and 336 h, respectively. V363A tau displayed a different pathway of assembly for intermediate species, which were more stable and defined; V363A also demonstrated a delay in the appearance of large aggregates (after 672 h of incubation).

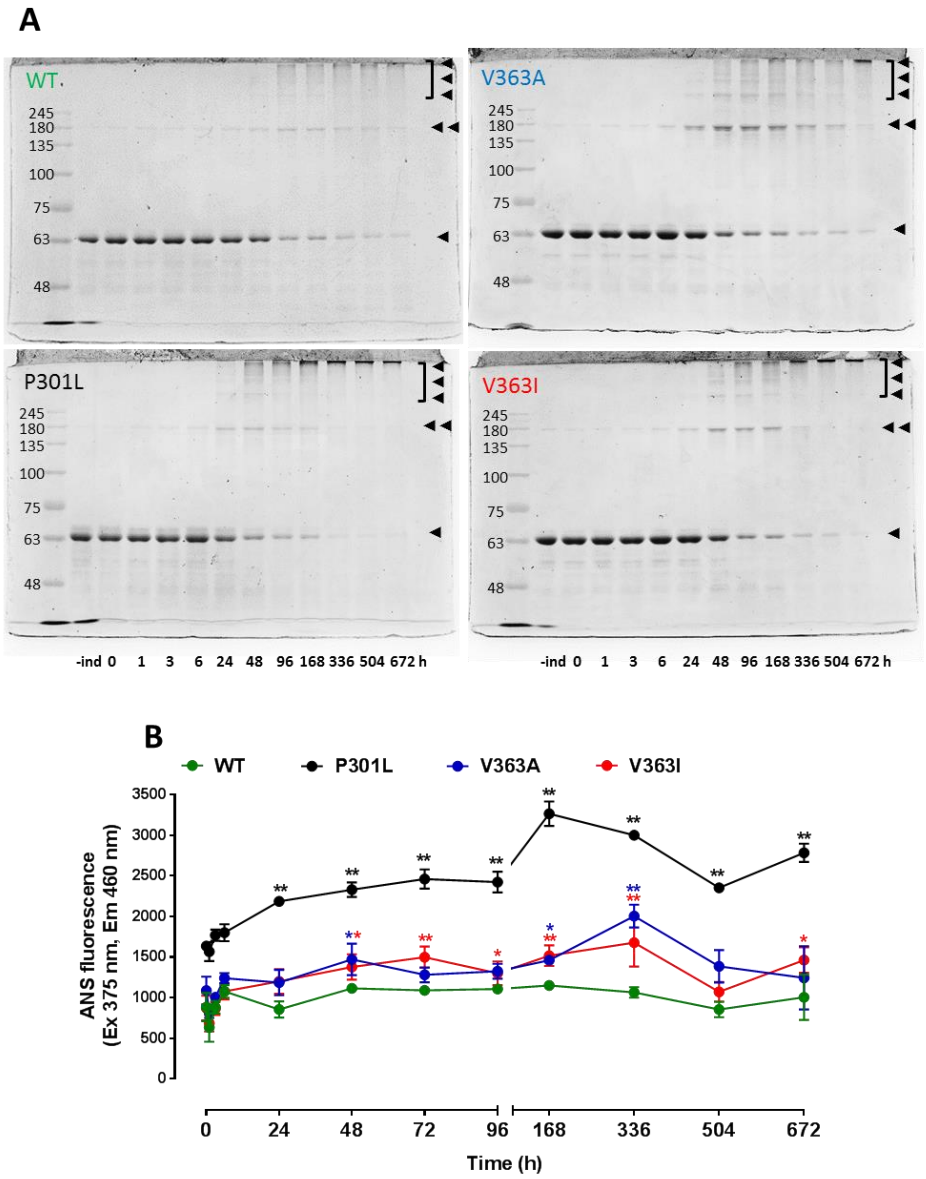

Figure 6. Aggregation process and hydrophobicity. (**A**) Semi-denaturing PAGE of samples obtained after long incubation times (from 0 to 672 h) in presence of heparin. Two µg of protein/lane of WT and mutated tau proteins were resolved in 8% polyacrylamide gels and stained with R-250 Coomassie blue. The first lane reports the molecular markers (MW, kDa). The (-ind) lane reports the sample without heparin. The following symbols are used: ◄ monomers (apparent MW 63 kDa), ◄◄

oligomers (apparent MW 180 kDa), and ◄◄◄ large aggregates (apparent MW > 245 kDa). (**B**) ANS-dependent fluorescence response. WT and mutated tau proteins (2 μM) incubated at 37°C in presence of heparin for different intervals of time were added to ANS (20 μM), and fluorescence emissions were measured. Data represent the mean ± standard error of eight replicates from two different experiments. One-way ANOVA and Dunnett's comparison test were used. *$p < 0.05$ and **$p < 0.01$ vs. t = 0 h.

To explore the pattern of hydrophobic residues, we used 8-anilino-1-naphthalene sulfonic acid (ANS, Fig. 6B). P301L tau was more hydrophobic than the other mutated proteins or WT tau from 24 h of incubation ($p < 0.01$ vs. t = 0), displaying a higher fluorescence intensity at all incubation times, with a maximum value reached after approximately 168 h. V363A and V363I tau demonstrated a similar tendency, with increased ANS fluorescence compared with WT tau, which was significantly higher for both V363 tau with respect to t = 0 h, but almost constant for all incubation times. A slight deviation towards a greater exposure of hydrophobic residues was observed at 168 h for V363I and at 336 h for V363A, although it was definitely lower than for P301L. Such a behavior was in agreement with the formation of transient intermediate species.

3.5 V363A and V363I tau toxicity

To verify the biological activity of tau mutant proteins, we applied samples from different incubation times to the human neuroblastoma SH-SY5Y cell line and assessed viability according to mitochondrial activity (Fig. 7).

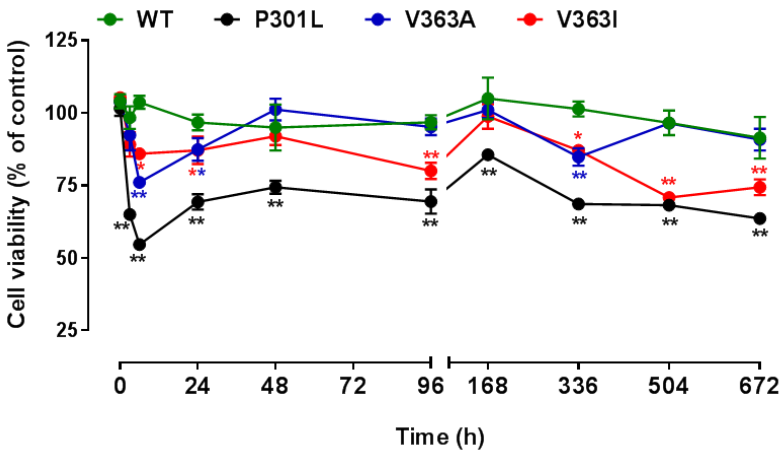

Figure 7. Cytotoxicity of WT and mutated tau proteins. SH-SY5Y neuroblastoma cell survival after 24 h of treatment with 1 µM of WT or mutated tau proteins after different incubation times (from 0 to 672 h), in presence of heparin. Data represent the mean ± standard error of 10 replicates from three different experiments. One-way ANOVA and Dunnett's comparison test were used. *$p < 0.05$ and **$p < 0.01$ vs. t = 0 h.

WT tau at 1 µM did not affect cell survival at any time point. As expected, P301L tau had significant toxicity effects at every time point, with variable toxicity (35% and 45% at 3 and 6 h, respectively, $p < 0.01$ vs. t = 0), which became nearly constant from 24 h to the longer incubation times (~35%, $p < 0.01$ vs. t = 0). V363A and V363I did not display a constant toxicity pattern. For short incubation times, at 6 h, V363A tau was more toxic than V363I tau (24% and 14%, $p < 0.01$ and $p < 0.05$, respectively vs. t = 0). At longer incubation times, the toxicity of V363A tau decreased, becoming less toxic than V363I tau, except for 336 h (15%, $p < 0.01$ vs. t = 0), similar to V363I tau (13%, $p < 0.05$ vs. t = 0), and similar to WT at 48h delay, with no significant toxic effect. Reversely, the toxicity of V363I tau increased over time (at 96 h, 20%, $p < 0.01$ vs. t = 0), similar to the effects observed for P301L tau (30% and 25% at 504 and 672 h, respectively, $p < 0.01$ vs. t = 0).. Overall, the mutated tau proteins' effectiveness in inducing cellular toxicity under our experimental conditions was confirmed for P301L tau, whereas the toxicities of V363A and V363I tau depended on the incubation times, the V363A being more effective at short times, while the V363I at long times.

4. Discussion

There is ample evidence supporting the hypothesis that tau mutations promote neurodegeneration, because by compromising physiological tau functions result in a risk factor for tauopathies. Tau mutations have also been associated with DNA damage and a predisposition to chromosome instability [31]. As an ubiquitous structural cytoplasmic neuronal protein, any alterations in tau can compromise various fundamental functions [32].

Tau is an intrinsically disordered protein, containing hydrophilic residues that define a limited secondary structure and high conformational flexibility. Full-length WT tau does not aggregate spontaneously under physiological conditions, and its propensity to polymerize is increased by the presence of point mutations, especially those in the microtubule-binding domain; this reduces the biological functions of tau and increases toxicity, such as the P301L. This mutation promotes β-sheet formation with faster kinetics, based on ThT and rapid aggregation assays, quite likely due to the elimination of proline-specific constraints and the exposure of aggregate-prone motifs [33–35].

The V363A and V363I tau mutations are close to the P364 belonging to the Pro-Gly-Gly-Gly sequence of the fourth microtubule-binding repeat (R4), that has the same pathological features of P301L [11]. The proximity of V363 mutations to the Pro-Gly-Gly-Gly sequence could explain the pathological features: V363A tau reduced and delayed the polymerization of tubulin, and both V363A and V363I had unusual aggregation properties [12].

The long-time schedule in our experimental conditions enabled us to observe the asymptotic aggregative behavior of full-length V363 mutated tau proteins in comparison with WT and P301L tau proteins and to observe interesting differences along their aggregation pathways. The unusual aggregation properties of both V363A and V363I could give structural hints in their pathological pathway.

As far as tau proteins are free in solution (monomeric form), mutations do not dramatically affect their conformation. In SAXS experiments, all tau proteins were detected as intrinsically disordered proteins with a similar radius of gyration. *Ab initio* modeling suggested that P301L tau monomers adopt a more compact shape in solution, while V363A and V363I tau have a more splayed structure, similar to the WT tau.

Differences emerged immediately after the addition of heparin. As expected, the P301L variant was more prone than WT tau to complexing. Reversely and unexpectedly, V363A and V363I tau did not form any supramolecular assemblies at this stage, suggesting that the one-to-one interaction occurred with heparin does not induce any sudden conformational change promoting further complexation. Also, the presence of these mutations' triggers - to different extents - the capacity to form aggregates during short- and long-term experimental conditions.

Assemblies formed by WT are amorphous and stable and the protein showed a low propensity to acquire a beta-sheet structure. Differently, V363A, and V363I mutations changed their conformation to the beta-sheet structure and gradually developed a similar fraction of complexes. Interestingly the conformational change was slower as compared both to the fast-and large change of P301L and also to the small change of WT.

Morphological analysis using AFM helped clarify the nature of the intermediate forms and describe globally the structures forming during incubation. A variety of forms and sizes were observed in the presence of mutated tau proteins, with P301L tau progressing to fibrillary structures faster than V363A and V363I tau. Under our experimental conditions, WT tau was less prone to aggregate in well-defined structures and only oligomeric or at most very short protofibrils were observed. P301L tau evolved from monomeric to fibrillary forms following a typical fast aggregation pathway, which was confirmed by ThT and ANS fluorescence assays. Interestingly, the V363A and V363I mutated tau displayed distinct patterns of aggregation, with persistent intermediate forms visible as shorter and less abundant fibrils at AFM and a more abundant 180-kDa band under Coomassie stain.

The definition of all tau species was only possible by applying a modification to the canonical SDS-PAGE process, which enabled us to verify the presence of aggregation intermediates. We did not do western blot analysis because aggregates at high molecular weights (more than 245 kDa) are generally lost during wet or semi-dry transfers from gels to membranes. Since the tau protein monomer was apparent at 63 kDa, the 180-kDa band might represent a trimeric form. However, this species has also been identified in patients' brain samples, and molecular mass analysis (Surface-enhanced laser desorption/ionization-time of flight mass spectrometry) indicated that this form was

dimeric [21]. Over very long times, the two V363 mutations diverge, the intermediate forms disappearing in V363I while still present in V363A.

Also cell toxicity, tested with neuroblastoma cells, appears to follow a parallel evolution. The toxicity of exogenous P301L tau tested on the neuroblastoma cell line was significant at all incubation times, associated with all the different protein species formed during incubation. By contrast, the V363A and V363I tau mutations affected cell viability differently with regard to intensity and timing. V363A is more toxic at the initial stages, then turning to a viability profile similar to WT, V363I, initially less toxic than V363A, slowly approaches the viability profile of P301L over very long times.

The effects of interactions between tau species and the extracellular matrix on neuroblastoma cell uptake have been documented (Frost, Michel) [19,36]In our experimental conditions, results on the mitochondrial metabolism, confirm that V363 tau were biologically active, with an effect modulated by the prevailing complexed specie. Cell treatment using the whole population of complexed species, without the selective production or purification, allow to mimic the scenario in transfected cells [37], without the heterogeneity associated with overexpression.

Our results extend the currently limited knowledge about V363A and V363I atypical tau mutations. Although in a recent cell-free assay, these mutated proteins did not display the ability to aggregate in response to seed-induced aggregation [38], we demonstrated, by complementary experimental techniques, the particular aggregation processes associated with the V363A and V363I tau mutations. We confirmed the partial overlap between V363A and V363I, highlighting the importance of *in vitro* analyses to define the biochemical characteristics of protein mutations and decipher their pathogenic roles. The identification of aggregation intermediates can corroborate the oligomeric hypothesis of tauopathies.

It was recently reported [39] that the sequence between residues 353 and 368, in the fourth repeat of the microtubule-binding domain of tau, although not provided itself with aggregation capacity, is rather implicated in tau complexation as a regulator, with a role in the early intermediate process of changing the conformation into heparin-induced fibrils.

In this scenario, we confirm and describe how point mutations affecting tau in the position 363 modulate the pathway and timing of tau complexation, parallel to tau toxicity, hypothesising that they

may interfere with the putative regulatory engagement of the embedding sequence, driving to pathology.

Author contributions

A. D. L., L. Colombo, A. B., F. T. and G. R.: conceptualization; A. D. L., L. Colombo, L. R.., L. Cantù, E. D. F., A. B., C. R. and S. C.: investigation; A. D. L., L. Colombo, E. D. F, and M. S.: writing-original draft; all authors: editing.

Acknowledgments

We thank the Fondazione Sacchetti, and ESRF and BM29 staff for beam-time and assistance and Sara Parabicoli for preliminary data analysis. E.D.F. thanks BIOMETRA Dept. for partial support (PSR2019_DEL_FAVERO).

Declaration of interests

The authors declare that they have no known competing financial interests or personal relationships that could have appeared to influence the work reported in this paper.

REFERENCES

[1] M.G. Spillantini, M. Goedert, Tau pathology and neurodegeneration, Lancet Neurol., 12 (2013) 609–622.

[2] G. Rossi, F. Tagliavini, Frontotemporal lobar degeneration: old knowledge and new insight into the pathogenetic mechanisms of tau mutations, Front. Aging Neurosci., 7 (2015) 192.

[3] J.M. Decker, L. Krüger, A. Sydow, F.J. Dennissen, Z. Siskova, E. Mandelkow, E.-M. Mandelkow, The Tau/A152T mutation, a risk factor for frontotemporal-spectrum disorders, leads to NR2B receptor-mediated excitotoxicity, EMBO Rep., 17 (2016) 552–569.

[4] M. Goedert, M.G. Spillantini, Propagation of Tau aggregates, Mol. Brain, 10 (2017) 18.

[5] R. Skrabana, J. Sevcik, M. Novak, Intrinsically Disordered Proteins in the Neurodegenerative Processes: Formation of Tau Protein Paired Helical Filaments and Their Analysis, Cell. Mol. Neurobiol., 26 (2006) 1083–1095.

[6] V. Daebel, S. Chinnathambi, J. Biernat, M. Schwalbe, B. Habenstein, A. Loquet, E. Akoury, K. Tepper, H. Müller, M. Baldus, C. Griesinger, M. Zweckstetter, E. Mandelkow, V. Vijayan, A. Lange, β-Sheet Core of Tau Paired Helical Filaments Revealed by Solid-State NMR, J. Am. Chem. Soc., 134 (2012) 13982–13989.

[7] S. Walker, O. Ullman, C.M. Stultz, Using Intramolecular Disulfide Bonds in Tau Protein to Deduce Structural Features of Aggregation-resistant Conformations*, J. Biol. Chem., 287 (2012) 9591–9600.

[8] K.H. Strang, C.L. Croft, Z.A. Sorrentino, P. Chakrabarty, T.E. Golde, B.I. Giasson, Distinct differences in prion-like seeding and aggregation between Tau protein variants provide mechanistic insights into tauopathies, J. Biol. Chem., 293 (2018) 4579.

[9] S.S. Mirra, J.R. Murrell, M. Gearing, M.G. Spillantini, M. Goedert, R.A. Crowther, A.I. Levey, R. Jones, J. Green, J.M. Shoffner, B.H. Wainer, M.L. Schmidt, J.Q. Trojanowski, B. Ghetti, Tau Pathology in a Family with Dementia and a P301L Mutation in Tau, J. Neuropathol. Exp. Neurol., 58 (1999) 335–345.

[10] S.S. Shafiei, M.J. Guerrero-Muñoz, D.L. Castillo-Carranza, Tau Oligomers: Cytotoxicity, Propagation, and Mitochondrial Damage, Front. Aging Neurosci., 9 (2017) 83.

[11] G. Rossi, A. Bastone, E. Piccoli, G. Mazzoleni, M. Morbin, A. Uggetti, G. Giaccone, S. Sperber, M. Beeg, M. Salmona, F. Tagliavini, New mutations in MAPT gene causing frontotemporal lobar degeneration: biochemical and structural characterization, Neurobiol. Aging, 33 (2012) 834.e1-834.e6.

[12] G. Rossi, A. Bastone, E. Piccoli, M. Morbin, G. Mazzoleni, V. Fugnanesi, M. Beeg, E.D. Favero, L. Cantù, S. Motta, E. Salsano, D. Pareyson, A. Erbetta, A.E. Elia, F.D. Sorbo, V. Silani, C. Morelli, M. Salmona, F. Tagliavini, Different mutations at V363 MAPT codon are associated with atypical clinical phenotypes and show unusual structural and functional features, Neurobiol. Aging, 35 (2014) 408–417.

[13] S. Ahmed, M.D. Fairen, M.S. Sabir, P. Pastor, J. Ding, L. Ispierto, A. Butala, C.M. Morris, C. Schulte, T. Gasser, E. Jabbari, O. Pletnikova, H.R. Morris, J. Troncoso, E. Gelpi, A. Pantelyat, S.W. Scholz, MAPT pV363I mutation: A rare cause of corticobasal degeneration, Neurol. Genet., 5 (2019) e347–e347.

[14] C.M. Cowan, S. Quraishe, A. Mudher, What is the pathological significance of tau oligomers?, Biochem. Soc. Trans., 40 (2012) 693–697.

[15] K. Flach, I. Hilbrich, A. Schiffmann, U. Gärtner, M. Krüger, M. Leonhardt, H. Waschipky, L. Wick, T. Arendt, M. Holzer, Tau Oligomers Impair Artificial Membrane Integrity and Cellular Viability*, J. Biol. Chem., 287 (2012) 43223–43233.

[16] P. Friedhoff, M. von Bergen, E.-M. Mandelkow, E. Mandelkow, Structure of tau protein and assembly into paired helical filaments, Biochim. Biophys. Acta BBA - Mol. Basis Dis., 1502 (2000) 122–132.

[17] S. Barghorn, E. Mandelkow, Toward a Unified Scheme for the Aggregation of Tau into Alzheimer Paired Helical Filaments, Biochemistry, 41 (2002) 14885–14896.

[18] C. Haase, J.T. Stieler, T. Arendt, M. Holzer, Pseudophosphorylation of tau protein alters its ability for self-aggregation, J. Neurochem., 88 (2004) 1509–1520.

[19] B. Frost, R.L. Jacks, M.I. Diamond, Propagation of Tau Misfolding from the Outside to the Inside of a Cell*, J. Biol. Chem., 284 (2009) 12845–12852.
[20] C.A. Lasagna-Reeves, D.L. Castillo-Carranza, M.J. Guerrero-Muñoz, G.R. Jackson, R. Kayed, Preparation and Characterization of Neurotoxic Tau Oligomers, Biochemistry, 49 (2010) 10039–10041.
[21] K.R. Patterson, C. Remmers, Y. Fu, S. Brooker, N.M. Kanaan, L. Vana, S. Ward, J.F. Reyes, K. Philibert, M.J. Glucksman, L.I. Binder, Characterization of Prefibrillar Tau Oligomers in Vitro and in Alzheimer Disease*, J. Biol. Chem., 286 (2011) 23063–23076.
[22] S. Kaniyappan, R.R. Chandupatla, E.-M. Mandelkow, E. Mandelkow, Extracellular low-n oligomers of tau cause selective synaptotoxicity without affecting cell viability, Alzheimers Dement., 13 (2017) 1270–1291.
[23] S. Maeda, Y. Sato, A. Takashima, Frontotemporal dementia with Parkinsonism linked to chromosome-17 mutations enhance tau oligomer formation, Neurobiol. Aging, 69 (2018) 26–32.
[24] M. Doucet, J.H. Cho, G. Alina, J. Bakker, W. Bouwman, P. Butler, K. Campbell, M. Gonzales, R. Heenan, A. Jackson, P. Juhas, S. King, P. Kienzle, J. Krzywon, A. Markvardsen, T. Nielsen, L. O'Driscoll, W. Potrzebowski, R. Ferraz Leal, T. Richter, et al., SasView version 421, Zenodo, 2019.
[25] D. Franke, M.V. Petoukhov, P.V. Konarev, A. Panjkovich, A. Tuukkanen, H.D.T. Mertens, A.G. Kikhney, N.R. Hajizadeh, J.M. Franklin, C.M. Jeffries, D.I. Svergun, ATSAS 28: a comprehensive data analysis suite for small-angle scattering from macromolecular solutions, J. Appl. Crystallogr., 50 (2017) 1212–1225.
[26] A.G. Kikhney, D.I. Svergun, A practical guide to small angle X-ray scattering (SAXS) of flexible and intrinsically disordered proteins, FEBS Lett., 589 (2015) 2570–2577.
[27] A.V. Shkumatov, S. Chinnathambi, E. Mandelkow, D.I. Svergun, Structural memory of natively unfolded tau protein detected by small-angle X-ray scattering, Proteins Struct. Funct. Bioinforma., 79 (2011) 2122–2131.
[28] A. Battisti, G. Ciasca, A. Grottesi, A. Tenenbaum, Thermal compaction of the intrinsically disordered protein tau: entropic, structural, and hydrophobic factors, Phys Chem Chem Phys, 19 (2017) 8435–8446.
[29] N. Sibille, A. Sillen, A. Leroy, J.-M. Wieruszeski, B. Mulloy, I. Landrieu, G. Lippens, Structural Impact of Heparin Binding to Full-Length Tau As Studied by NMR Spectroscopy, Biochemistry, 45 (2006) 12560–12572.
[30] J. Zhao, I. Huvent, G. Lippens, D. Eliezer, A. Zhang, Q. Li, P. Tessier, R.J. Linhardt, F. Zhang, C. Wang, Glycan Determinants of Heparin-Tau Interaction, Biophys. J., 112 (2017) 921–932.
[31] G. Rossi, V. Redaelli, P. Contiero, S. Fabiano, G. Tagliabue, P. Perego, L. Benussi, A.C. Bruni, G. Filippini, M. Farinotti, G. Giaccone, S. Buiatiotis, C. Manzoni, R. Ferrari, F. Tagliavini, Tau Mutations Serve as a Novel Risk Factor for Cancer, Cancer Res., 78 (2018) 3731–3739.
[32] T.E. Tracy, L. Gan, Tau-mediated synaptic and neuronal dysfunction in neurodegenerative disease, Curr. Opin. Neurobiol., 51 (2018) 134–138.
[33] S. Barghorn, Q. Zheng-Fischhöfer, M. Ackmann, J. Biernat, M. von Bergen, E.-M. Mandelkow, E. Mandelkow, Structure, Microtubule Interactions, and Paired Helical Filament Aggregation by Tau Mutants of Frontotemporal Dementias, Biochemistry, 39 (2000) 11714–11721.
[34] H. Aoyagi, M. Hasegawa, A. Tamaoka, Fibrillogenic Nuclei Composed of P301L Mutant Tau Induce Elongation of P301L Tau but Not Wild-type Tau*, J. Biol. Chem., 282 (2007) 20309–20318.
[35] D. Chen, K.W. Drombosky, Z. Hou, L. Sari, O.M. Kashmer, B.D. Ryder, V.A. Perez, D.R. Woodard, M.M. Lin, M.I. Diamond, L.A. Joachimiak, Tau local structure shields an amyloid-forming motif and controls aggregation propensity, Nat. Commun., 10 (2019) 2493.
[36] C.H. Michel, S. Kumar, D. Pinotsi, A. Tunnacliffe, P.S. George-Hyslop, E. Mandelkow, E.-M. Mandelkow, C.F. Kaminski, G.S.K. Schierle, Extracellular Monomeric Tau Protein Is Sufficient to Initiate the Spread of Tau Protein Pathology*, J. Biol. Chem., 289 (2014) 956–967.

[37] M. Pickhardt, J. Biernat, S. Hübschmann, F.J.A. Dennissen, T. Timm, A. Aho, E.-M. Mandelkow, E. Mandelkow, Time course of Tau toxicity and pharmacologic prevention in a cell model of Tauopathy, Neurobiol. Aging, 57 (2017) 47–63.
[38] Y. Xia, Z.A. Sorrentino, J.D. Kim, K.H. Strang, C.J. Riffe, B.I. Giasson, Impaired tau–microtubule interactions are prevalent among pathogenic tau variants arising from missense mutations, J. Biol. Chem., 294 (2019) 18488–18503.
[39] S. Shimonaka, S.-E. Matsumoto, M. Elahi, K. Ishiguro, M. Hasegawa, N. Hattori, Y. Motoi, Asparagine residue 368 is involved in Alzheimer's disease tau strain–specific aggregation, J. Biol. Chem., 295 (2020) 13996–14014.